1 Introduction

Bisphosphonic acids are widely used in the pharmaceutical industry as drugs for degenerative bone disease or as ligand/chelating components thereof. It has been found that different functionalities in the bisphosphonate result in different potencies and this is a direct result of the conformational interaction of the bisphosphonate with the surface of the bone. The study focused on using various theoretical and spectroscopic methods to investigate the nature of the conformations in the aqueous medium, as well as at the bone mineral surface/liquid interface, for the reference bisphosphonate, 1-hydroxyethylidene-1,1-diphosphonic acid. This chapter provides an introduction to the system investigated, the techniques used to study the various conformers and bone mineral surface interaction.

1.1 Bisphosphonates

Bisphosphonates are compounds analogous to the naturally occurring pyrophosphate class of compounds and contain a P-C-P linkage, instead of a P-O-P linkage, as can be seen in Figure 1-1. The first use of bisphosphonates was mainly of an industrial nature and, most importantly, as 'water softeners' in domestic and industrial water systems due to their ability to inhibit the formation of insoluble calcium carbonate [1]. Pyrophosphates were determined to be calcification inhibitors [2] but efforts to utilise this property in the treatment of certain human conditions were unsuccessful due to pyrophosphates being hydrolysed under such physiological circumstances [1]. Attempts were made to find other compounds with similar inhibitory properties. Since bisphosphonates are resistant to hydrolysis and also have a high affinity for bone mineral, they proved to be the most successful alternative. These compounds were especially desirable because they were active when orally administered to rats [1, 3].

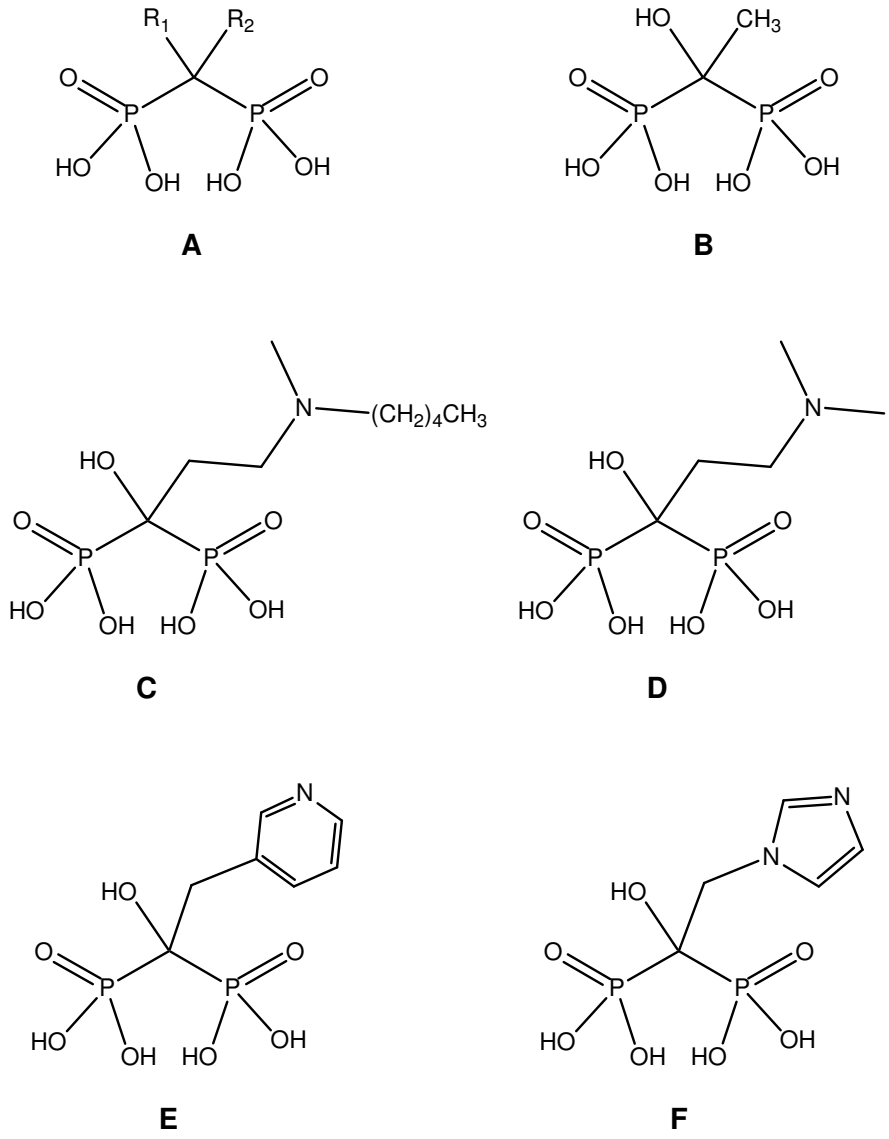

Figure 1-1. A. The generalised structure of the bisphosphonates and that of B. HEDP, C. ibandronic acid, D. olpadronic acid, E. risedronic acid and F. zoledronic acid

As the value of bisphosphonates with potential medical applications grew, the need to understand the relationships between structure and activity became more important, and various modifications to the bisphosphonate motif were investigated by varying the substituents R_1 and R_2 (Figure 1-1A). It was determined in early studies that the P-C-P moiety is integral to the high affinity of bisphosphonates for bone [1] and this high affinity was found to be significantly enhanced when R_1 = OH. The oldest, best known and benchmark bisphosphonate is 1-hydroxyethylidene-1,1-diphosphonic acid, in which R_1 = OH

and R_2 = CH_3 (Figure 1-1B). It is commonly abbreviated as HEDP and is commercially known as etidronic acid.

The high affinity of the bisphosphonates for bone mineral is not necessarily the only reason why they are potent antiresorption agents. Varying the R_2 side chain with R_1 = OH (Figure 1-1) showed that R_2 groups containing especially tertiary nitrogen atoms, such as ibandronic and olpadronic acid (Figures 1-1C and 1-1D), were much more potent than HEDP. The most potent of these groups were those in which the nitrogen was included in a heterocyclic ring, such as in risedronic and zoledronic acid (Figures 1-1E and 1-1F), being more than 10 000 times more potent than HEDP [1]. The presence of the two phosphonic acid groups is very important for the biological activity of the bisphosphonates and studies show that replacement of one or two of the phosphonic hydroxyl groups dramatically reduces both bone affinity and antiresorptivity in the molecule [1].

Thus, in summary, the presence of the two phosphonic groups as well as a hydroxyl group at R_1 is responsible for the high affinity for bone mineral and the targeting thereof. The antiresorptivity is mostly a function of the R_2 side chain and the three-dimensional conformation of the bisphosphonate at the bone mineral surface [1]. Comparisons of the activity of stereoisomers of certain bisphosphonates show a tenfold preference for one over the other, indicating the stereochemical preference of a possible receptor site [4]. This underlines the importance of understanding the structural aspects of these bisphosphonates on a more fundamental level, both that of the free molecule and that of the molecule at the bone mineral surface.

It would be meaningful, therefore, to begin such a study by focusing first on the benchmark bisphosphonate HEDP.

1.2 Radiopharmaceutical uses of bisphosphonates

The high affinity of bisphosphonates for bone mineral also suggests that these compounds should be ideal ligands for complexation with radionuclides for the

purpose of specifically targeting pain-palliative, imaging and chemotherapeutic treatments for bone cancer and its symptoms [1, 5, 6]. The radionuclide to be used should be a medium-energy β-emitter with prolonged, selective uptake and retention at the sites of infection [5]. Due to different radionuclides having different physiological behaviours in the body, this selectivity can be tuned by choosing an appropriate complexing ligand. Changed ligands with the same radionuclide can make them selective to different organs in the body [7].

The most commonly used radionuclides ^{186}Re and ^{99m}Tc and, recently, ^{177}Lu have been evaluated with promising results [6]. Other radionuclides, such as ^{153}Sm, ^{166}Ho and ^{117m}Sn, are also commonly used for various applications, but they are complexed with ligands containing different phosphorous based groups [5,6].

1.3 HEDP properties

HEDP, like most other bisphosphonates, is a tetraprotic acid and therefore has various forms having different degrees of protonation, such as H_4L, H_3L^-, H_2L^{2-}, HL^{3-}, L^{4-} where L = $[CH_3C(OH)(PO_3)_2]^{4-}$, that are pH-dependent and whose dissociation constants, pK_a, have been experimentally determined [8] (Table 1-1).

Table 1-1. The dissociation constants of HEDP [8].

Equilibrium reaction	Dissociation constant, pK_a
$H_4L \leftrightarrows H_3L^- + H^+$	2.43
$H_3L^- \leftrightarrows H_2L^{2-} + H^+$	2.97
$H_2L^{2-} \leftrightarrows HL^{3-} + H^+$	6.81
$HL^{3-} \leftrightarrows L^{4-} + H^+$	10.11

HEDP has a high affinity for complexation with metal ions and especially divalent ions, as evidenced from the approximately 23 single-crystal structures that have been reported [9]. As a solid, HEDP crystallises as a monohydrate, but an anhydrous crystalline form also exists above 70 ºC as evidenced by the X-ray diffraction (XRD) powder pattern [10].

To understand the three-dimensional interaction of a bisphosphonate with a surface/interface, it is important to fundamentally investigate the structural aspects of the molecule in its various degrees of protonation and its interaction with bone minerals. As the accepted benchmark molecule in the bisphosphonate family, HEDP would therefore be the logical starting point for a study using various complementary spectroscopic methods, each with its own strengths and weaknesses.

1.4 Hydroxyapatite as a model of bone

Natural bone is a poorly crystalline hydroxyapatite (HA) with the general composition of ±65% w/w mineral component, of which the HA has a crystallinity index of ±35 and is 7.4% carbonated [11]. The rest of the bone matrix is made up mainly of organic compounds (25%) and water (10%) [11]. Synthetic HA, $Ca_{10}(PO_4)_6(OH)_2$, has been used to substitute mineral bone in drug interaction studies, and many other calcium phosphitic compounds have been used extensively in the biological and medical fields for bone replacement or as mimicking agents [11]. HA has been compared with fluorinated, carbonated and biological apatites by means of Raman and IR spectroscopy [12-16] and powder diffraction methods [17, 18]. The main properties of HA have been shown to be similar to those of biological bone apatite. Due to the incorporation of carbonate [18] and thus the absence of OH in the crystal structure [16] of biological bone, it has been found that the interactions of bisphosphonates with bone and synthetic HA may differ [19]. However, chemical interactions have been shown to be very similar for HEDP with both bovine bone and synthetic HA, and therefore HA is still a viable substitute for biological bone in fundamental research [20]. Nevertheless, great care should be taken in the interpretation and extrapolation of interaction results.

1.5 Spectroscopic methods

The various techniques used in this study were chosen for their ability to contribute unique aspects to the understanding of and insight into the conformations of HEDP both in solution and in the solid state, as well as to its behaviour at the solid-solution interface.

NMR spectroscopy was chosen to investigate how pH affects the chemical nature of HEDP as chemical shifts are sensitive to both environmental changes (the solution) and chemical changes (deprotonation of the phosphonate groups) in the molecule. As the chemical shift in this study is a function of pH, the NMR data can also be used to monitor the degree of deprotonation of HEDP.

X-ray diffraction was chosen to investigate the solid-state aspects of HEDP as knowledge of the nature of molecular conformation and interaction in the solid state can be used to compare and rationalise what is observed in solution. Three-dimensional structural data can be obtained from both single crystal and powder XRD techniques. The preferred method is single crystal, but in many cases it is not possible to obtain good-quality single crystals and powder diffraction data are then analysed using the Rietveld method to determine the crystal structure, as in the case of anhydrous HEDP.

Vibrational spectroscopy is a unique technique for giving insight into local internal changes (being of a physical or chemical nature) in a molecule or to the intra/intermolecular interactions of molecules. This is done by analysing the shift or appearance/disappearance of the vibrational bands associated with the molecule of interest in the solid and/or solution phases. Raman spectroscopy is ideally suited to studying molecular interactions at the surface of a solid substrate and will therefore give insight into the interaction of HEDP with HA as a model of bone. Raman spectroscopy is also ideally suited for studying aqueous systems as water is a weak Raman scatterer, while infrared spectroscopy is ideal for observing changes associated with water molecules, as required during the dehydration of HEDP in the solid state. Thus, vibrational techniques will give

great insight into conformers and their interactions, both in the solid state and in solution.

1.5.1 Nuclear magnetic resonance (NMR) spectroscopy

The most important property for an atomic nucleus to be NMR-active is the nuclear spin, I, which can have values of $0 + \frac{1}{2}n$, where n is an element of the natural numbers, in units of $h/2\pi$ [21]. Values of $I = 0$ are indicative of NMR-inactive nuclei. Each nucleus has an associated proportionality constant, γ, called the 'magnetogyric ratio' associated with the nuclear magnetic moment, μ, which is directly proportional to the spin. This relationship can be written as:

$$\mu = \frac{\gamma I h}{2\pi} \tag{1.1}$$

By application of an external magnetic field, the nuclear moments can align themselves in $2I + 1$ orientations having a magnetic quantum number, m_I, with values of $-I, -I + 1, \ldots, I - 1, I$ and this interaction energy for each orientation can be written as [21]:

$$E = -\frac{\gamma h}{2\pi} m_I B \tag{1.2}$$

The NMR selection rules allow for a transition to have $\Delta m_I = \pm 1$, and thus the transition energy is:

$$\Delta E = \left| E_{m_{I+1}} - E_{m_I} \right|$$

$$\Delta E = \frac{\gamma h B}{2\pi} \tag{1.3}$$

from Eq. 1.2.

To detect this transition, external radiation must be applied such that the energy of this radiation, $h\nu$, equals ΔE. Substituting ΔE in Eq. 1.3 for $h\nu$ gives the fundamental resonance condition for the NMR experiment as:

$$\nu = \frac{\gamma B}{2\pi} \tag{1.4}$$

The relative resonance frequency of the fundamental resonance condition for an atomic nucleus in an NMR experiment depends mostly on its magnetic environment, and therefore on the variation in electron density (from chemical bonds and neighbouring atoms) of each nucleus [22]. Measuring this resonance frequency in conjunction with the spin-spin coupling of the nuclei will, in general, allow the determination of at least the connectivity of simple molecules. Comparative NMR spectra will also show whether the chemical environment/character of an atomic nucleus has changed significantly due to a chemical modification to either the environment (change in pH) or the molecule itself (ligand coordination).

In this study the ^{1}H, ^{13}C, ^{31}P and ^{23}Na NMR spectra of HEDP, in the monohydrate and anhydrous forms, as well as the calcium dihydrate salt, were investigated in DMSO-d_6, D_2O and H_2O as solvents to monitor and compare the various structural and conformational changes that occurred in a solution environment.

1.5.2 X-ray diffraction (XRD)

The diffraction of X-rays by the crystal lattice allows the determination of the molecular structure of solids. This requires knowledge of the atoms in a regular crystal system, the lattice parameters and the relative positions and intensities of reflections. Systematic absences of certain families of hkl reflections from the diffraction data allows the assignment of space groups or at least suggests a number of possible space groups to investigate. The condition for diffraction is mathematically described by Bragg's law:

$$2d_{hkl}\sin\theta = n\lambda \quad (n \in N) \tag{1.5}$$

where d_{hkl} is the spacing for the hkl plane, θ the scattering or reflection angle between the radiation and the hkl plane, and n the order of the diffraction [23] . This is graphically represented in Figure 1-2.

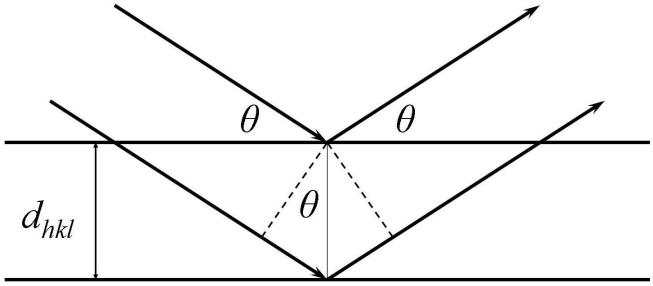

Figure 1-2. Schematic of X-ray diffraction from an hkl lattice plane, with interplanar distance d_{hkl} and diffraction angle θ [23]

1.5.2.1 Single-crystal XRD

Diffraction occurs in a crystal when Bragg's law is satisfied and the structure factor for the reflection, F_{hkl}, can be related to the measured intensity of that hkl plane's diffraction, I_{hkl}, as:

$$I_{hkl} = \left|F_{hkl}\right|^2 \tag{1.6}$$

F_{hkl} can be written as an imaginary function:

$$F_{hkl} = \sum_{j=1}^{N} f_j e^{2\pi i(hx_j+ky_j+lz_j)} \tag{1.7}$$

in which all N atoms, with fractional coordinates x, y and z, in the lattice contribute to an hkl plane, including the atomic scattering factor, f_j, for each atom type, j [23]. F_{hkl} is related to the electron density function, ρ_{xyz}, by the use of a Fourier transformation:

$$\rho_{xyz} = \frac{1}{V} \sum_{h,k,l=-\infty}^{+\infty} F_{hkl} e^{-2\pi i(hx+ky+lz)} \tag{1.8}$$

in which the maxima of ρ_{xyz} correspond to the atomic positions, and thus the crystal structure is solved [23]. A problem arises in the experimental data as seen in Eq. 1.6 when the phase information is not available. Successful methods to solve this problem are well established [23], but will not be discussed here. However, it is worth noting that the validity of the solutions involves the calculation of an R-factor, which is in general defined as:

$$R = \left(\frac{\sum \left| |F_{obs}| - |F_{calc}| \right|}{\sum |F_{obs}|} \right) \tag{1.9}$$

for all reflections. The smaller the value of R, the better the solution fit for the structure.

1.5.2.2 Powder XRD

The complexity of using powder XRD data for crystal structure determination stems from the fact that with this method diffraction is observed as a 'cone' due to the many randomly orientated crystallites, and thus three-dimensional data are compressed into one dimension [24]. Further complications arise from the fact that the data profile and the quality of data required are extremely dependent on the instrumentation, as evidenced by the number of factors that are weighted when attempting to solve an XRD powder pattern [24]. The structural solution of an XRD powder pattern follows a very similar method to that for single-crystal XRD, in which indexing, crystal system and lattice parameter determination, and space group identification become intrinsically more difficult due to the compression of the three-dimensional data into one dimension [24]. The most popular and effective method utilised at various stages of such an analysis is the Rietveld method [24], which will be discussed in more detail in Section 1.6.3.

Even though it would appear that attempting the solution of a crystal structure by utilising powder XRD data is extremely labour-intensive, it is the best method in the absence of single-crystal data of diffraction quality.

1.5.3 Vibrational spectroscopy

The energy of a molecule can be summarised as one of four components:

$$E_T = E_{trans} + E_{e^-} + E_{vib} + E_{rot} \tag{1.10}$$

The study of the vibrational energy associated with a molecule, E_{vib}, uses the two complementary techniques of infrared (IR) and Raman spectroscopy. A very comprehensive review of these two techniques and their applications can be found in reference [25] – only a concise synopsis of the two techniques is presented here. The relationship between IR and all Raman processes is shown schematically in Figure 1-3.

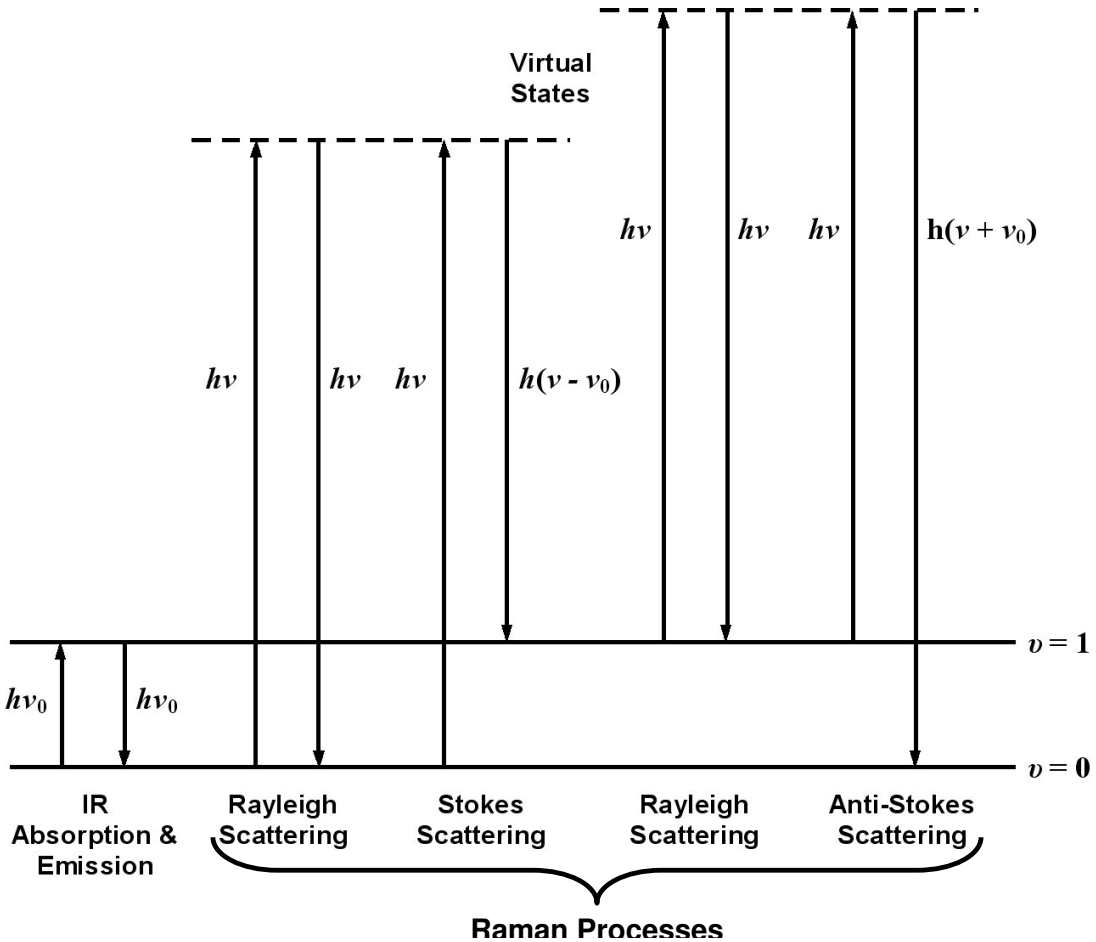

Figure 1-3. Schematic showing the difference between the various vibrational processes

1.5.3.1 Infrared (IR) spectroscopy

IR spectra originate from the absorption of a photon between two vibrational energy levels. In general, a vibrational mode is IR-active when the dipole moment, μ, associated with the mode is non-zero. From quantum mechanics it is shown that molecular vibrational energy levels are quantised and that the dipole moment of an associated vibration will couple with the electric field of the IR radiation, ν_{IR}, only when the associated energy of this IR radiation matches that of a specific vibrational energy level of the molecule, allowing the absorption and emission of IR photons by vibrational energy levels in the molecule's electronic ground state [26]. The frequency measured during IR absorption can be formulated as being:

$$\nu_{IR} = \frac{d\mu}{dx} \tag{1.11}$$

which describes the change of the permanent dipole moment, $d\mu$, as the molecule vibrates, dx.

1.5.3.2 Raman spectroscopy

Raman spectroscopy is a scattering technique during which a sample is irradiated with a single wavelength source (i.e. a laser) and electronic polarisation is induced in the dipole associated with a vibrational mode. Three scattering processes can occur when the sample is irradiated: Rayleigh, Stokes and anti-Stokes scattering. Rayleigh scattering occurs when the frequency of the scattered radiation equals that of the incoming radiation [26]. When the scattered radiation's frequency differs from that of the incident radiation, Stokes/anti-Stokes scattering occurs and it is the frequency difference between the incident and scattered radiation that is of interest to the spectroscopist. From classical theory these processes can be summarised as:

$$\mu_i = \alpha_0 E_0 \cos 2\pi\nu t + \frac{1}{2}\left(\frac{\partial\alpha}{\partial x}\right)_0 x_0 E_0 \{\cos[2\pi(\nu+\nu_0)t] + \cos[2\pi(\nu-\nu_0)t]\} \tag{1.12}$$

where the first term describes Rayleigh scattering and the last term the anti-Stokes ($\nu + \nu_0$) and Stokes ($\nu - \nu_0$) scattering [26] with the induced dipole moment, μ_i, dependent on the polarisability, α. In practice, Stokes scattering is mostly measured because it originates from the $\upsilon = 0$ vibrational level which is more populated than the $\upsilon = 1$ level from where the anti-Stokes scattering originates (see Figure 1-3), as described by the Boltzman distribution of these levels at ambient temperatures [26].

1.6 Molecular modelling

Molecular modelling is used to assist with and/or confirm many aspects of experimental chemistry. If the theory is an acceptable description of the system of interest, a wealth of information can be obtained theoretically, which would usually be very time-consuming to obtain experimentally. In the case of HEDP, the vibrational spectra are complex and many ambiguous, overlapping bands are observed, making empirical assignment very difficult. Calculation of the theoretical spectra can therefore be used to confidently identify and confirm bands that can be associated with chemical or conformational changes, as well as the associated intra/intermolecular interactions.

1.6.1 The theoretical method

Two main methods are used in molecular modelling: molecular mechanics (MM), which is based on the laws of classical physics, and the electronic structure method, which is based on quantum mechanics [27]. The latter can be divided into semi-empirical, *ab initio* and density functional theory (DFT); the most widely used of these is the DFT method which takes the effects of electron correlation into account [27]. The DFT method is very similar to the *ab initio* Hartree-Fock (HF) method, but here the electron is assumed to interact with an 'averaged electron density' [27].

In the DFT method, the electronic energy, E^e, can be seen as a summation of the electrons' kinetic energy, E^t, the potential energy of the nuclear-electron interaction, E^v, the electron-electron repulsion energy, E^j, and the exchange correlation term, E^{xc}, that describes the rest of the electron-electron interactions [27]:

$$E^e = E^t + E^v + E^j + E^{xc} \tag{1.13}$$

It is the numerical integration evaluation of the E^{xc} term that makes DFT the superior method to HF, but at the cost of calculation complexity. The E^{xc} term is a functional of the electron density function, ρ, and can be separated into the exchange and correlation functionals, $E^x(\rho)$ and $E^c(\rho)$, respectively:

$$E^{xc}(\rho) = E^x(\rho) + E^c(\rho) \tag{1.14}$$

A pure DFT functional (E^{xc}) is usually defined by pairing an exchange functional with a correlation functional as in the case of the BLYP functional where a Becke (B) defined functional (E^x) is combined with a Lee-Yang-Parr (LYP) functional (E^c) [27].

DFT hybrid functionals have also been defined where the E^{xc} term contains an HF-type E^x term contribution as HF theory contains an E^x term as part of its own formulation [27]. Thus,

$$E^{xc}_{hybrid} = c_{HF} E^x_{HF} + c_{DFT} E^{xc}_{DFT} \tag{1.15}$$

where the c's are constants. As an example, the classical B3LYP hybrid exchange-correlation functional could be defined as:

$$E^{xc}_{B3LYP} = E^x_{LDA} + c_0\left(E^x_{HF} - E^x_{LDA}\right) + c_x \Delta E^x_{B88} + E^c_{VWN3} + c_c\left(E^c_{LYP} - E^c_{VWN3}\right) \tag{1.16}$$

where LDA, B88 and VWN3 and LYP are all exchange or correlation functionals defined in the literature [27].

1.6.2 Basis sets

For a theoretical calculation it is also necessary to describe mathematically the orbitals that combine to approximate the total electronic wavefunction of the system under investigation [27]. Better orbital descriptions implies larger basis sets, which lead to longer calculation times being required.

There are three main ways to enlarge the description of an atomic orbital:

(1) Create split-valence basis sets in which two or more basis functions describe the same orbital, although these descriptions will differ in size. One can also have triple split-valence sets which use three contracted descriptions for each orbital type. An example of such a basis set is 6-311 [27].

(2) Introduce polarisation functions into the basis sets that describe the orbitals, with angular momentum beyond the ground-state description for the atom, such as p-orbital functions to s-orbital descriptions or d-orbital functions to p-orbital descriptions. This can be justified by arguing that because molecules are not a grouping of non-interacting separate atoms, a better description of the orbitals can be obtained by describing a possible change in shape of the atomic orbitals [27]. Their addition is indicated in brackets (a,b), where a indicates the function added to heavy atoms and b the function added to hydrogen atoms. Basis sets with higher angular momentum have more than one type of function added to either heavy or hydrogen atoms and can even have more than one of the same type of function added, indicated by a numerical coefficient in the bracket, e.g. (2df,3pd).

3) Enlarge the basis set by adding diffuse functions to the orbital description, which allows larger versions of the s- and p-orbital types. This is important for systems in which the electrons are further than normal from the nucleus, e.g. where there are lone pairs present or the system is anionic in nature [27]. In the basis set description, “+” denotes that diffuse functions are added only to heavy atoms, and “++” denotes that diffuse functions are

added to hydrogen atoms as well [27]. A graphical summary with examples of basis sets of all these effects is given in Table 1-2.

Table 1-2. Graphical representation of the different effects that can be added to expand the basis set used during molecular modelling [27]

Basis set effects	Graphical representation	Basis set examples
Split valency	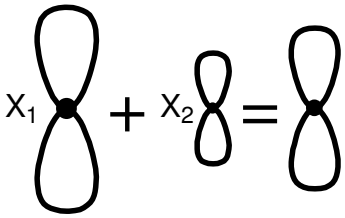	3-21G 6-31G 6-311G
Polarisation	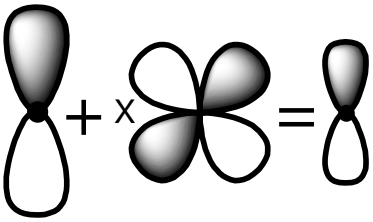	3-21G(d) 6-31G(d,p) 6-311(2df,3pd)
Diffuseness	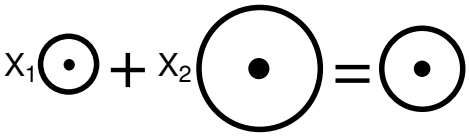	6-31G+(d,p) 6-311++(2df,3pd)

1.6.3 The Rietveld method

The Rietveld method is said to be the most powerful method for extracting solid-state structural information on a compound from experimentally obtained powder XRD patterns, and is based on the deceptively simple rationale of minimising parameters such that the residual quantity

$$S_y = \sum_{i=1}^{i} w_i \left(y_i - y_{ci}\right)^2 \qquad (1.17)$$

approximates zero during the least-squares refinement [24], where y_i and y_{ci} are the observed and calculated intensities at the ith step of the powder pattern, respectively, and $w_i = 1/y_i$. The complexity of the Rietveld method only becomes

apparent when the calculated intensity, y_{ci}, for the ith step is defined with all the necessary parameters during the refinement process:

$$y_{ci} = s \sum_{h,k,l=-\infty}^{\infty} L_{hkl} \left| F_{hkl} \right|^2 \phi(2\theta_i - 2\theta_{hkl}) P_{hkl} A + y_{bi} \tag{1.18}$$

The variables L_{hkl}, F_{hkl} and P_{hkl} are all separate functions for an hkl reflection, as allowed by Bragg's law (Eq. 1.5), defining the Lorentz, polarisation and multiplicity factors, the structure factor (similar to Eq. 1.7) and the preferred orientation function respectively [24]. s is a scaling factor, ϕ the reflection profile function, A the absorption factor and y_{bi} the background intensity at the ith step defined at least as a 5th order polynomial [24]. All of the factors and functions are instrument- and/or sample-dependent, and this is where the real complexity and difficulty of Rietveld refinement is experienced.

As with the single XRD case, Rietveld refinement has certain criteria of fit that have the same function as Eq. 1.9. As a result of so many variables having to be optimised simultaneously, various criteria of fit have been defined, of which the following are important: the R-structure factor

$$R_F = \frac{\sum \left| \sqrt{I_{K-observed}} - \sqrt{I_{K-calculated}} \right|}{\sum \sqrt{I_{K-observed}}} \tag{1.19}$$

the R-Bragg factor

$$R_B = \frac{\sum \left| I_{K-observed} - I_{K-calculated} \right|}{\sum I_{K-observed}} \tag{1.20}$$

the R-pattern

$$R_p = \frac{\sum \left| y_i - y_{ic} \right|}{\sum y_i} \tag{1.21}$$

and the R-weighted pattern

$$R_{wp} = \sqrt{\frac{\sum w_i (y_i - y_{ic})^2}{\sum w_i (y_i)^2}} \qquad (1.22)$$

R_{wp} and R_B are most often used, but all the criteria are examined to decide whether the structure solution is valid as it can be seriously inflated by external factors such as sample impurity or can be deflated by factors such as significantly high background profiles [24].

1.7 Aim

The general use of bisphosphonates in bone degenerative diseases has been outlined, as well as the techniques and methods employed in this thesis. Very little is known about the interactions of bisphosphonates with bone on a fundamental, molecular as indicated by an analysis of available literature. Therefore the need exists for a more fundamental study of these compounds. HEDP is the oldest known, benchmark and chemically simplest bisphosphonate and would therefore be the most logical point to start such an investigation using hydroxyapatite as a simplified model for bone.

In all fundamental studies the validation of both theoretical and experimental methods are important. Therefore many relevant spectroscopic techniques as earlier described were used and the experimental data rationalised by theoretical calculations / methods.

It is therefore the aim of this thesis to investigate the interaction of HEDP with hydroxyapatite as a model of bone on a fundamental level using these various techniques for future extension and methodology development to study other bisphosphonates and solution/solid interaction environments more relevant to cancerous environments in the human body.

1.8 References

[1] R.G.G. Russell. *Ann. N.Y. Acad. Sci.* **2006**, *1068*, 367.

[2] H.A. Fleisch, R.G.G. Russell, F. Straumann. *Clin. Sci.* **1966**, *31*, 461.

[3] H.A. Fleisch, R.G.G. Russell, S. Bisaz, R.C. Mühlbauer, D.A. Williams. *Eur. J. Clin. Invest.* **1970**, *1*, 12.

[4] H.A. Fleisch. *Endocr. Rev.* **1998**, ***19***, 80.

[5] V.J. Lewington. *Phys. Med. Biol.* **1996**, *41*, 2027.

[6] V. Lungu, D. Niculae, P. Bouziotis, I. Pirmettis, C. Podina. *J. Radioanal. Nucl. Ch.* **2007**, *273*, 663.

[7] J.R. Zeevaart. *Metal-ion Speciation in Blood Plasma as a Tool in Predicting the in vivo Behaviour of Potential Bone-seeking Radiopharmaceuticals*, Delft University Press, Delft, **2001**, Chapter 1.

[8] J.R. Zeevaart, N.V. Jarvis, I. Cukrowski, G.E. Jackson. *S. Afr. J. Chem.* **1997**, *50*, 189.

[9] J.P. Silvestre, N.Q. Dao, Y. Leroux. *Heteroatom Chem.* **2001**, *12*, 73.

[10] E.G. Afonin, G.G. Aleksandrov. *Russ. J. Gen. Chem.* **2003**, *73*, 340.

[11] S.G. Dorozhkin, M. Epple. *Angew. Chem. Int. Ed.* **2002**, *41*, 3130.

[12] M.A. Walters, Y.C. Lang, N.C. Blumenthal, R.Z. le Geros, I.L.A. Konsker. *J. Inorg. Biochem.* **1990**, *39*, 193.

[13] G. Penel, G. Leroy, C. Rey, B. Sombret, J.P. Huvenne, E. Bres. *J. Mater. Sci – Mater. M.* **1997**, *8*, 271.

[14] G. Penel, C. Delfossea, M. Descamps, G. Leroy. *Bone* **2005**, *36*, 893.

[15] A. Antonakos, E. Liarokapis, T. Leventouri. *Biomaterials* **2007**, *28*, 3043.

[16] J.D. Pasteris, B. Wopenka, J.J. Freeman, K. Rogers, E. Valsami-Jones, J.A.M. van der Houwen, M.J. Silva. *Biomaterials* **2004**, *25*, 229.

[17] T. Leventouri, B.C. Chakoumakos, N. Papaneachou, V. Perdikatsis. *J. Mater. Res.* **2001**, *16*, 2600.

[18] T. Leventouri. *Biomaterials* **2006**, *27*, 3339.

[19] G.H. Nancollas, R. Tang, R.J. Phipps, Z. Henneman, S. Gulde, W. Wu, A. Mangood, R.G.G. Russell, F.H. Ebetino. *Bone* **2006**, *38*, 617.

[20] I. Cukrowski, L. Popović, W. Barnard, S.O. Paul, P.H. van Rooyen, D.C. Liles. *Bone* **2007**, *41*, 668.

[21] R.J. Abraham, J. Fisher, P. Loftus. *Introduction to NMR Spectroscopy,* 2nd Edition, John Wiley & Sons, Chichester, **1988**, Chapter 1.

[22] D.H. Williams, I. Fleming. *Spectroscopic Methods in Organic Chemistry,* 5th Edition, McGraw-Hill, Bath, **1995**, Chapter 3.

[23] C. Giacovazzo (Ed.). *Fundamentals of Crystallography*, Oxford University Press, Oxford, **1992**, Chapter 3.

[24] R.A. Young (Ed.). *The Rietveld Method*, Oxford University Press, Oxford, **1996**.

[25] J.M. Chalmers, P.R. Griffiths. *Handbook of Vibrational Spectroscopy,* 2nd Edition, John Wiley & Sons, Chichester, **2002**, all volumes.

[26] K. Nakamoto. *Infrared and Raman Spectra of Inorganic and Coordination Compounds,* 5th Edition, John Wiley & Sons, Chichester, **1997**, Part A.

[27] J.B. Foresman, Æ. Frisch. *Exploring Chemistry with Electronic Structure Methods,* 2nd Edition, Gaussian Inc., Pittsburgh, **1996**.

2 Experimental

2.1 Introduction

This chapter contains the necessary information for the description of each experiment performed to study the surface interactions of HEDP(aq), as well as HEDP in solution and in the solid state. The choice of each of the main techniques has been discussed in Chapter 1. These techniques are all necessary to obtain a global view of the surface interactions of HEDP, as well as to characterise HEDP itself and in solution.

2.2 Chemicals

HEDP was purchased from Fluka >97% and Dayang Chemicals >99%, and used as is for the preparation of the 0.5 M solutions and for solid-state investigations. The monohydrate form of HEDP was obtained by recrystallisation from deionised, distilled water, and the anhydrous form was obtained by heating HEDP at 120 ºC to ensure that all water of hydration and all adsorbed water was removed [1]. $Ca(OH)_2$ ≥ 95% and H_3PO_4 (85% in H_2O) were purchased from Sigma-Aldrich and hydroxyapatite (BIO-RAD, BIO-GEL®-HTP Gel) was obtained from Chemlab, Bryanston, South Africa.

$CaHPO_4$ was prepared by adding 3 g of $Ca(OH)_2$ to 4.86 ml of a 5 M phosphoric acid solution at boiling point, after which the desired product precipitated and was filtered, washed with distilled water and dried overnight at 120 ℃ [2]. The calcium dihydrate salt of HEDP, $Ca(CH_3C(OH)(PO_3H)_2)\cdot 2H_2O$ ($CaH_2L\cdot 2H_2O$), was prepared by adding $Ca(OH)_2$ to an HEDP solution in the molar ratio of 1:1. The desired product immediately precipitates out as it is only sparingly soluble at higher pH values and this precipitated complex was filtered and washed with deionised water and left to air-dry overnight [2]. The single crystal used for XRD

analysis was grown from a solution containing 25 mg of HA dissolved in 0.5 M of HEDP [2]. The bovine bone used was obtained from a local abattoir and treated with H_2O_2 and acetone [2] to remove as much of the organic component as possible.

The pH series of solutions used for the ^{31}P NMR study and Raman spectra Multivariate Curve Resolution analysis were prepared by titrating an initial solution of 20 ml of 0.5 M HEDP with a 0.5 M NaOH solution using a Metrohm 765 Dosimat autotitrator, that was calibrated by the two point calibration method. Sampling was done at pH intervals of 0.20 close to the equivalence points or at intervals of 0.50 away from them. This resulted in a sample set of 50 different pH values over the pH range 0.98 – 13.00. Each sample was placed in a separate NMR tube and used for both the NMR and FT-Raman analyses.

2.3 NMR spectroscopy

The NMR spectra of HEDP monohydrate ($H_4L{\cdot}H_2O$) and the anhydrous (H_4L) forms, as well as $CaH_2L{\cdot}2H_2O$, were obtained with DMSO-d_6 and D_2O as solvents. The spectra of the NaOH-titrated solutions were measured in H_2O as solvent.

2.3.1 ^{1}H and ^{13}C nuclei

The ^{1}H and ^{13}C spectra measured in DMSO-d_6 were referenced to the deuterated DMSO itself at 2.49 and 39.5 ppm respectively. All ^{1}H and ^{13}C measurements in D_2O and H_2O were referenced using an internal standard probe of $CDCl_3$ having saturation-recovery (SR) values of 4 100.56 Hz for the ^{1}H and –1 928.13 Hz for the ^{13}C data. All ^{1}H and ^{13}C spectra were measured on a Bruker ARX-300 spectrometer at 300.135 and 75.469 MHz respectively.

2.3.2 ^{31}P and ^{23}Na nuclei

All ^{31}P spectra were measured on a Bruker ARX-300 spectrometer at 121.46 MHz and referenced to 85% H_3PO_4 in H_2O at 0.00 ppm. The ^{23}Na data were collected at 132.26 MHz on a Bruker AVANCE-500 spectrometer and referenced to 1.0 M NaBr in H_2O.

2.4 Thermal gravimetric analysis

Data for HEDP·H_2O were collected using a Mettler/Toledo TGA/SDT851^e instrument. Thermal events were registered under a nitrogen atmosphere, in the range 25 – 300 ºC, with the temperature gradient set to 10 ºC per minute.

2.5 X-ray diffraction methods

2.5.1 Single-crystal X-ray diffraction

The single X-ray crystal structure analysis was performed using data collected at 20 ºC on a Siemens P4 diffractometer fitted with a Bruker 1K CCD detector and SMART control software [3] using graphite-monochromated, Mo-Kα radiation by means of a combination of ϕ and ω scans. Data reduction was performed using SAINT+ [3] and the intensities were corrected for absorption using SADABS [3]. The structure was solved by direct methods using SHELXTS [3] and refined by full-matrix least squares using SHELXTL [3] and SHELXL-97 [4].

All the hydrogen atoms were located experimentally and were included in the refinement. For the determination of $CaH_2L{\cdot}2H_2O$ (Figure 3-12A), a half-occupancy was assigned to the H5 and H6 atoms, which represent a disordered hydroxyl group bonded to P2, and equally distributed between O5 and O6. Also, H5 and H6 were allowed to ride on O5 and O6 respectively with $d_{O–H}$ = 0.82(1) Å, and the P-O–H angle made tetrahedral and allowed to rotate about the corresponding O-P bond. The isotropic displacement parameters of H5 and H6 were fixed at 1.5 times the equivalent isotropic displacement parameters of O5

and O6 respectively. The crystal data and refinement tables for $H_4L{\cdot}H_2O$ and $CaH_2L{\cdot}2H_2O$ can be found in Tables A-1 and A-2 in the Appendix.

Perspective drawings of the structures of $H_4L{\cdot}H_2O$ and $CaH_2L{\cdot}2H_2O$ were produced using Ortep-3 for Windows (version 1.076) [5], Mercury (version 1.4.2) [6] and POV-Ray for Windows (version 3.6) [7].

2.5.2 Powder X-ray diffraction

The powder XRD analysis was performed using a PANalytical X-pert Pro powder diffractometer with variable divergence and receiving slits, and an X'celerator detector using Fe-filtered Co-Kα radiation. Data were collected over the 2θ angle range of 5.0 – 90.0º. Data collection for H_4L was performed using an Anton Paar HTK 16 heating chamber with a Pt-heating strip both at room temperature and at 120 ºC, with a waiting time of 30 minutes at 120 ºC before data accumulation commenced. For the Rietveld refinement procedure, Y_2O_3 annealed at 1 200 ºC was also measured as a reference for instrument parameter refinement.

2.6 Rietveld refinement

The instrument parameters were refined by using the powder pattern of annealed Y_2O_3 as reference; the unit cell constants' parameters were kept constant and the instrument parameters were allowed to refine. All indexing and refinement procedures were done using the TOPAS Academic [8] software package.

The powder X-ray diffraction pattern of anhydrous HEDP was indexed and a Pawley [9] and Le Bail [10] fitting for the 2θ range 5 – 45º done for comparison, during which the cell parameters were refined using the instrument profile as obtained from the Y_2O_3 refinement. Structure determination was attempted using a 'first guess' rigid-body description of HEDP obtained from the known $HEDP{\cdot}H_2O$ structure which contained only the non-hydrogen atoms for the 2θ range 5 – 45º. After the best fit had been obtained by means of the rigid-body refinement procedure, all non-hydrogen atomic positions were allowed to be

refined independently until an optimal and acceptable R-value was obtained with a molecular solution that also made chemical sense.

2.7 Molecular modelling

Structural optimisations and vibrational spectra calculations were performed using Gaussian03 software [11], employing the 6-311++G(d,p) basis set unless otherwise stated.

For the calculation of the vibrational spectra of $CaH_2L \cdot 2H_2O$, the starting conformation coordinates from the crystallographic structure solution were used without further structural optimisation, and one full unit cell was necessary to reproduce the vibrational spectrum satisfactorily. The Hartree-Fock (HF/6-311++G(d,p)) level of theory was selected, based on initial evaluation of similar, simple systems modelled with analogous Density Functional Theory (DFT) which showed satisfactory comparisons for the region below 2000 cm^{-1}. The scaling factor used was determined to be 0.9051 [12].

Conformers of the various protonated forms of HEDP (H_3L^-, H_2L^{2-}, HL^{3-}, L^{4-}) in solution were generated from the known single-crystal structure of $H_4L \cdot H_2O$ [13]. Initial solvated, conformers for H_4L were generated using Macromodel 9.6207 of the Schrödinger Software Suite, utilising the MM/OPLS-2005 force field. The default solvation settings in Macromodel were used. All conformers of interest were then further optimised using the Gaussian03 software [11] performing the DFT calculations at the B3LYP/6-311++G(d,p) level of theory in conjunction with the SCRF IEF-PCM/UA0 solvation model. Final validity of all generated conformers during this very preliminary conformational analysis was based on the generation of imaginary frequencies during the final DFT calculations.

The hybrid functional B3LYP was selected, as it is widely used in literature and gives acceptable results regarding structural properties. It was decided to add diffusion functions (++), as ionic systems are also being modelled. The polarisation functions (d,p) were added to both non-hydrogen and hydrogen

atoms to ensure a better modelling of hydrogen bond interaction in the molecule(s). The solvation model as well as all other settings are default for the Gaussian03 package and are well known to give acceptable results.

2.8 Vibrational spectroscopy

2.8.1 Raman spectroscopy

Various experimental solid-state and solution Raman spectra were obtained using both a dispersive and an FT-Raman spectrometer.

All dispersive spectra were obtained by exciting the samples with the 514.5 nm (green) line of a Coherent Innova 300 Argon-ion laser. For the solid-state spectra, an Olympus confocal microscope with a 50X objective was used to focus the laser light on the sample or at a solid-liquid interface. The scattered light was dispersed and recorded by means of a Dilor XY multichannel Raman spectrometer equipped with a liquid nitrogen-cooled Wright Generation 1 CCD detector. The spectral resolution was 3 cm^{-1}, while laser output power at the source (300 – 500 mW) and integration times (30 – 120 seconds) was varied to obtain the best possible spectra. Three to four spectral accumulations were averaged, and the software used for data processing was Labspec 3.03.

A Linkam RMS 90 heating cell was employed to obtain the solid-state Raman spectrum for non-ambient conditions at 120 ºC, and the macro-Raman solution spectra on the dispersive system were obtained in an NMR tube using a 50 mm lens in a 180º backscattering geometry. The *in situ* Raman measurements that were done to monitor the interaction of HEDP with bone, HA and $CaHPO_4$ were performed on the dispersive instrument using the confocal microscope, by adding HEDP solution (0.5 – 0.005 M) onto solid HA or $CaHPO_4$ (on a microscope slide) and sequentially recording the Raman spectra until no further change was observed.

The FT-Raman spectra of the HEDP solutions were obtained in NMR tubes by using a Bruker IFS 100 FT-Raman spectrometer fitted with a liquid N_2-cooled Ge detector. All solid-state spectra were measured directly on the surface of the solid. All spectra were recorded for the region 100 – 3500 cm^{-1} using the 1 064 nm excitation line of an Nd:YAG laser operating at approximately 300 mW at the sample. The spectral resolution was 4 cm^{-1} and the spectra were signal-averaged over 128 – 512 scans as required, and processed using OPUS 5.5 software.

2.8.2 Fourier transform infrared (FTIR) spectroscopy

FTIR spectra were obtained under vacuum as a 1% w/w KBr disk using a Bruker IFS 113 spectrometer over the region 400 – 4000 cm^{-1} with a spectral resolution of 4 cm^{-1}. OPUS 5.5 software was used for data processing. The FTIR spectrum for HEDP at 120 ºC was obtained by heating the KBr pellet at 120 ºC for two hours, after which the pellet was immediately transferred to the spectrometer for spectral accumulation under vacuum.

2.9 Multivariate Curve Resolution (MCR)

The MCR routine of The Unscrambler® version 9.6 (CAMO Process AS, Oslo, Norway) was used for the pure component analysis of the bands in the wavenumber range 860 – 1280 cm^{-1}. This range was specifically chosen to include only those vibrational bands associated with the PO_3H_2 moieties. Non-negativity (for concentration values) and unimodality constraints were included for certain of the MCR analyses as required. The experimental spectra were modified with baseline offset and linear baseline correction before the MCR analysis commenced.

2.10 References

[1] E.G. Afonin, G.G. Aleksandrov. *Russ. J. Gen. Chem.* **2003**, *73*, 340.

[2] I. Cukrowski, L. Popović, W. Barnard, S.O. Paul, P.H. van Rooyen, D.C. Liles. *Bone* **2007**, *41*, 668.

[3] SMART (Version 5.054), SAINT (Version 6.45), SADABS (Version 2.10) and SHELXTS/SHELXTL (Version 6.12). Bruker AXS Inc., Madison, Wisconsin, USA, **2001**.

[4] SHELXS-97 and SHELXL-97. Sheldrick, GM University of Göttingen, Germany, **1997**.

[5] L.J. Faruggia. *J. Appl Crystallogr*. **1997**, *30*, 565.

[6] Mercury (Version 1.4.2). Cambridge Crystallographic Data Centre, http://www.ccdc.cam.ac.uk, **2007**.

[7] POV-Ray for Windows. (Version 3.6) Persistence of Vision Raytracer (Pty) Ltd., Victoria, Australia, http://www.povray.org, **2004**.

[8] A.A. Coelho, *J. Appl. Cryst.* **2000**, *33*, 899.

[9] G.S. Pawley. *J. Appl. Crystallogr.* **1981**, *14*, 357.

[10] A. Le Bail, H. Duroy, J.L. Fourquet. *Mater. Res. Bull.* **1988**, *23*, 447.

[11] M.J. Frisch, G.W. Trucks, H.B. Schlegel, G.E. Scuseria, M.A. Robb, J.R. Cheeseman, J.A. Montgomery, T. Vreven, K.N. Kudin, J.C. Burant, J.M. Millam, S.S. Iyengar, J. Tomasi, V. Barone, B. Mennucci, M. Cossi, G. Scalmani, N. Rega, G.A. Petersson, H. Nakatsuji, M. Hada, M. Ehara, K. Toyota, R. Fukuda, J. Hasegawa, M. Ishida, T. Nakajima, Y. Honda, O. Kitao, H. Nakai, M. Klene, X. Li, J.E. Knox, H.P. Hratchian, J.B. Cross, V. Bakken, C. Adamo, J. Jaramillo, R. Gomperts, R.E. Stratmann, O. Yazyev, A.J. Austin, R. Cammi, C. Pomelli, J.W. Ochterski, P.Y. Ayala, K. Morokuma, G.A. Voth, P. Salvador, J.J. Dannenberg, V.G. Zakrzewski, S. Dapprich, A.D. Daniels, M.C. Strain, O. Farkas, D.K. Malick, A.D. Rabuck, K. Raghavachari, J.B. Foresman, J.V. Ortiz, Q. Cui, A.G. Baboul, S. Clifford, J. Cioslowski, B.B. Stefanov, G. Liu, A. Liashenko, P. Piskorz, I. Komamori, R.L. Martin, D.J. Fox, T. Keith, M.A. Al-Laham, C.Y. Peng, A. Nanayakkara, M. Challacombe, P.M.W. Gill, B. Johnson, W. Chen, M.W. Wong, C. Gonzalez, J.A. Pople. Gaussian03, Revision D.01, **2004**.

[12] A.P. Scott, L. Radom. *J. Phys. Chem*. **1996**, *100*, 16502.

[13] J.P. Silvestre, N.Q. Dao, G. Heger, A. Cousson. *Phosphorus Sulphur* **2002**, *177*, 277.